# Conformational Analysis of d($C_3G_3$), a B-Family Duplex in Solution†

Steven Wolk, William N. Thurmes, Wilson S. Ross, Charles C. Hardin, and Ignacio Tinoco, Jr.*
*Department of Chemistry and Laboratory of Chemical Biodynamics, University of California, Berkeley, California 94720*
*Received June 9, 1988; Revised Manuscript Received November 15, 1988*

ABSTRACT: NMR and circular dichroism studies of the duplex formed by the self-complementary DNA hexanucleotide d($C_3G_3$) indicate that it is a B-type structure but differs from standard B-form. An analysis of NMR coupling constants within the deoxyribose moieties yields a 70% or greater contribution from pseudorotation phase angles corresponding to the C3′-exo conformation, a conformation similar to the C2′-endo conformation associated with B-form DNA. Intranucleotide interproton distances are consistent with a B-form structure, but some internucleotide distances are intermediate between A- and B-form structures. Circular dichroism spectra have B-form characteristics but also include an unusual negative band at 282 nm. The solution spectroscopic results are in contrast with X-ray crystallographic studies which find A-form structures for similar sequences.

Sequence-specific structural heterogeneity within Watson–Crick base-paired double-helical molecules is well established (Wells et al., 1979; Patel et al., 1982; Calladine, 1982). DNA sequences of the type $dC_n \cdot dG_n$, which have been proposed to adopt an unusual helical conformation, are of particular interest. Several studies (Simpson & Künzler, 1979; Rhodes, 1979) reported that poly(dG)·poly(dC) will not associate with histones to form chromatin-like structures under conditions where both poly(dA-dT)·poly(dA-dT) and poly(dG-dC)·poly(dG-dC) do. Nishimura et al. (1985) presented Raman spectroscopy evidence that poly(dG)·poly(dC) is in the A-form at high concentrations (0.2 M in base pairs) and in the B-form at low concentrations (0.01 M). This result was confirmed by Benevides et al. (1986), who found that this polymer is in an A-form in a 4% solution and a B-form in a 2% solution. These authors also studied d(CCCCGGGG) by X-ray and Raman methods and found that it has mixed 2′-endo (B-type) and 3′-endo (A-type) deoxyribose conformations in a crystal. A-form crystal structures have been reported for d(CCGG) (Conner et al., 1982), d(GGGGCCCC) (McCall et al., 1985), d(GCCCGGGC) (Heinemann et al., 1987), and d(CCCCGGGG) (Haran et al., 1987). Wang et al. (1982) obtained a modified A-form crystal structure for dGGCCGGCC in which the central four bases had A-type stacking but B-type sugar conformations.

Because of the apparent differences in structure induced by high nucleic acid concentrations, and possibly by crystal packing forces and the nonaqueous solvents used to induce crystal formation, it is worthwhile to study the solution structure of these sequences by NMR. The self-complementary sequence d(CCCGGG) was selected primarily due to its short length and 2-fold axis of symmetry, both of which simplify a potentially crowded $^1H$ NMR spectrum.

Although present NMR methods do not allow the direct measurement of global helical parameters, certain key differences between the A- and B-forms are detectable. The deoxyribose conformation is C2′-endo in B-form and C3′-endo in A-form (Saenger, 1984). Since this conformational shift is accompanied by a change in dihedral angles, the proton–proton scalar coupling constant magnitudes, $J$, are very sensitive to sugar conformation (Karplus, 1959; de Leeuw & Altona, 1982). Thus, in principle, all of the coupling constants within the deoxyribose ring can be used to deduce the pseudorotation phase angles $P$ that characterize the sugar conformations. Only couplings between H1′, H2′, H2″, and H3′ were measured and used in our analysis. Many interproton distances also change, and most distances shorter than 5 Å are measurable by NOE[1] experiments. These distances allow estimation of $P$, the glycosidic torsion angle $\chi$, and base stacking, all of which differ in the A and B conformations.

## Materials and Methods

The DNA oligonucleotide d(CCCGGG) was synthesized by standard solid-phase phosphoramidite methods on a DNA synthesizer designed by Dr. James Williamson (Chemistry Department, Stanford University). The product was purified by strong anion-exchange HPLC on a preparative Whatman Partisil 10 SAX column, using a linear gradient from 50 mM $NH_4OAc$ to 2 M $NH_4OAc$ in 20% EtOH over 20 min.

The RNA oligonucleotide r(CCCGGG) was synthesized by phosphoramidite solid-support methods using the following protocols: The protected nucleosides were synthesized according to the procedures in Markiewicz et al. (1984), with minor modifications. Guanosine was N-protected with the isobutyryl group (Ti et al., 1982). The phosphoramidites were prepared by treatment of the protected monomers with excess (β-cyanoethoxy)(*N*,*N*-diisopropylamino)chlorophosphine, which was quenched with benzyl alcohol. The phosphoramidites were then purified by flash chromatography on Merck 230–400 mesh silica gel using a hexane/acetone/triethylamine solvent mixture. Derivatized silica gel was prepared and the oligonucleotide assembled by a solid-phase method described in Kierzek (1986). After deprotection, the oligonucleotide was purified by HPLC on Nucleogen DEAE 60-7 using a gradient of 20 mM–1 M triethylammonium acetate in 20% acetonitrile over 60 min. This salt was removed by lyophilization. To prepare a sample for NMR study, residual triethylammonium was removed by addition of ammonium acetate and subsequent lyophilization.

All NMR data were obtained in 100 mM NaCl, 10 mM sodium phosphate, pH 7, and 1 mM EDTA at 18 °C. The

† This work was supported by National Institutes of Health Grant GM 10840 (I.T.) and the U.S. Department of Energy Office of Energy Research, under contract DE-FG03-86ER60406 (I.T.). C.C.H. was supported by NIH–NRSA Postdoctoral Fellowship GM 11638.

[1] Abbreviations: CD, circular dichroism; COSY, correlated spectroscopy; EDTA, ethylenediaminetetraacetic acid; FID, free induction decay; NOE, nuclear Overhauser effect; NOESY, nuclear Overhauser effect spectroscopy; TFE, trifluoroethanol; TMP, trimethyl phosphate; TPPI, time-proportional phase incrementation; TSP, sodium 3-(trimethylsilyl)-1-propanesulfonate.

0006-2960/89/0428-2452$01.50/0 

d($C_3G_3$) concentration was 3 mM, and the r($C_3G_3$) concentration was 0.6 mM. NMR samples were prepared by combining the nucleic acid with 0.4 mL of buffer, lyophilizing repeatedly from 99.8% $D_2O$ (Cambridge Isotope Laboratories), resuspending in 0.4 mL of 99.96% $D_2O$ under $N_2$, and placing in a 5-mM NMR tube (Aldrich, gold label). Partially deuterated sodium 3-(trimethylsilyl)-1-propanesulfonate (TSP) was used as the internal $^1H$ chemical shift reference. All NMR data were collected on a General Electric GN-500 spectrometer or a Bruker AM-500 spectrometer equipped with an Aspect 3000 computer.

One-dimensional spectra were collected in 16K data sets. 64 scans were acquired for DNA samples, and 1956 scans were taken for the RNA sample. Decoupling experiments were performed on the Bruker instrument by using the standard homonuclear decoupling pulse program.

Two-dimensional phase-sensitive NOESY and COSY spectra were collected by using standard pulse sequences (Ernst et al., 1987) and TPPI phase cycling (Bodenhausen et al., 1984). NOESY data sets (2K points) were collected for each of 400 $t_1$ values, with 80 scans per $t_1$. The relaxation delay between scans was 6 s for the first series of experiments (mixing times of 100, 200, 350, 500, and 800 ms) and 2 s for the second series (mixing times of 35, 70, and 105 ms). Data were transferred via magnetic tape to either a VAX 11/785 or a MicroVAX computer and processed by using software kindly provided by Dr. Dennis Hare. All data sets were Fourier transformed in the $t_2$ dimension, zero filled, and transformed in the $t_1$ dimension, yielding 1K by 1K data sets. Data were not apodized in $t_2$ and were apodized in $t_1$ by a 90° phase-shifted sine bell which decayed to zero at the end of the data points. Prior to Fourier transformation, the first row of data were multiplied by 0.5 (Otting et al., 1986) and the first column was multiplied by 2.1 (empirically determined) to reduce ridges in the transformed data sets.

NOESY cross-peaks were integrated by using the elliptical fit routine provided with the processing software. Cross-peak radius values ($r_{row}$,$r_{col}$) were chosen by each of two methods. First, the radii were measured as half of the width of the peak at the base in the row and column containing maximum amplitude for the particular cross-peak. A $j$ value (the software subroutine command for cross-peak radii) was then chosen which produced radii values that most closely matched the values measured in the rows and columns. Second, $j$ values were chosen which drew an ellipse that most closely fit (by visual inspection) the base of cross-peak. In all cases tested, the distance value obtained by either method was the same within experimental error.

COSY data sets (4K) were collected for 800 $t_1$ values with 32 scans per $t_1$ and a 2-s delay between scans. The data set was apodized by an unshifted sine bell which decayed to zero at the end of the data points and was zero filled in both dimensions to yield a 4K by 4K data set for improved digital resolution.

Circular dichroism spectra were collected on a Jasco J600 spectropolarimeter interfaced to an IBM PC. Samples were maintained at constant temperature in a 1-cm path length cylindrical cell surrounded by an external jacket for water circulation. Absorbance measurements were made on a Shimadzu UV-160 spectrophotometer. Oligonucleotide concentrations in CD experiments were approximately 20 $\mu$M. The concentration of the sample in TFE was not corrected for contributions from single strands. All CD and absorbance measurements were base line corrected for signals arising from the cell and buffer.

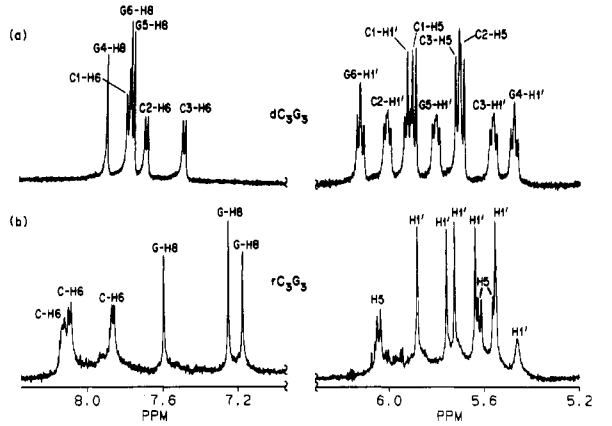


FIGURE 1: Aromatic and H2′,H2″ regions of the 500-MHz proton NMR spectrum of (a) d($C_3G_3$) and (b) r($C_3G_3$) in 100 mM NaCl and 10 mM sodium phosphate, pH 7, 18 °C.

Initial structures for molecular mechanics studies were generated by the NUCGEN module of AMBER (Kollman et al., 1981) and were based on Langridge B-form DNA and Arnott A-form RNA, with hydrogen atoms substituted for the 2′-hydroxyl groups in the latter form. Sugar groups in the initial structures were manually replaced with sugars having different puckers by using the INSIGHT graphics program on an Evans & Sutherland PS300 workstation. The unmodified and modified structures were energy-minimized by the conjugate gradient method with AMBER, using the force field described in Weiner et al. (1983). An energy gradient of less than $10^{-7}$ kcal $mol^{-1}$ $step^{-1}$ was used as the convergence criterion. A distance-dependent dielectric constant ($\epsilon = R_{ij}$) was used to simulate the presence of water (Kollman et al., 1981).

The pseudorotation phase angle ($P$) of the puckers in the minimized structures were determined with the AMBER analysis module using the PUCKER option. The helical axis displacement [$D$; see Saenger (1984)] was measured on the graphics screen by constructing a line connecting the guanine C8 and the cytosine C6 atoms, then measuring the perpendicular distance between the line and an approximate helical axis, and scaling the measurement by comparison with a known value.

## RESULTS

*NMR Spectrum and Peak Assignments.* Portions of the one-dimensional NMR spectrum of d(CCCGGG)·d(CCCGGG) [referred to as d($C_3G_3$)] in 100 mM NaCl buffer at 18 °C are shown in Figure 1. One peak is found for each proton, which indicates that the molecule exists in one average structure, as opposed to a slowly exchanging aggregate of nonequivalent strands. Aromatic resonances (GH8 and CH6) and deoxyribose H1′ protons were assigned by using the standard H6/8($n$) ↔ H1′($n$) ↔ H6/8($n$+1) NOE connectivity path. Deoxyribose H2′, H2″, H3′, and H4′ resonances were assigned by successive COSY connectivities and confirmed by the appropriate cross-peak patterns in several different regions of a NOESY spectrum obtained with a 100-ms mixing time. The deoxyribose H5′ and H5″ resonances were not assigned. This assignment method has been described in great detail elsewhere (Hare et al., 1983). The assigned chemical shift values are listed in Table I.

Figure 1 also shows the aromatic and H1′/H5 region of r($C_3G_3$) along with the same regions of the d($C_3G_3$) measured under identical buffer conditions. The GH8 resonances in the RNA spectrum are upfield from the CH6 resonances, while the reverse is true in the DNA spectrum. This demonstrates a difference in the stacking of neighboring residues in the two forms. Ring current effects from neighboring bases are known

Table I: Chemical Shifts[a] of the Assigned Resonances of 3 mM $d(C_3G_3)$ in 100 mM NaCl, 10 mM Sodium Phosphate, pH 7, and 1 mM EDTA at 18 °C

| | C1 | C2 | C3 | G4 | G5 | G6 |
|---|---|---|---|---|---|---|
| H6 | 7.78 | 7.68 | 7.48 | | | |
| H5 | 5.88 | 5.68 | 5.71 | | | |
| H8 | | | | 7.89 | 7.77 | 7.75 |
| H1′ | 5.91 | 6.00 | 5.55 | 5.47 | 5.80 | 6.11 |
| H2′ | 2.19 | 2.24 | 2.05 | 2.72 | 2.64 | 2.53 |
| H2″ | 2.56 | 2.48 | 2.35 | 2.72 | 2.78 | 2.39 |
| H3′ | 4.67 | 4.87 | 4.87 | 5.00 | 5.02 | 4.67 |
| H4′ | 4.13 | 4.24 | 4.14 | 4.36 | 4.43 | 4.23 |

[a] In ppm relative to TSP.

to cause small upfield changes in chemical shift (Geissner-Prettre & Pullman, 1970, 1976). In the A-form crystal structure of $d(G_4C_4)$ (McCall et al., 1985), adjacent guanosine residues are stacked with the five-membered ring of guanine over the six-membered ring of the neighboring cytosine. Also, the cytosine residues in the crystal structure show very little overlap. Since guanosines generate stronger ring currents than cytosines (Geissner-Prettre & Pullman, 1976), this is consistent with an A-form solution structure in $r(C_3G_3)$, as expected. This also indicates that $d(C_3G_3)$ has a stacking arrangement that is not similar to that of the A-form.

*Coupling Constant Analysis.* The values of vicinal proton–proton coupling constants within a deoxyribose moiety have been shown to be a sensitive measure of the average conformation, which can be described in terms of a pseudorotation phase angle ($P$) (Altona & Sundaralingam, 1972). Thus, various coupling constants and sums of coupling constants were measured by using standard decoupling experiments and a phase-sensitive COSY experiment. A sum of coupling constants represents a sum of all the splittings of a particular resonance and can be measured by the width between the outermost peaks of the multiplet. For example, the H2′ resonance is split by coupling to the H1′, H2″, and H3′ protons. Therefore, $J_{\Sigma 2'} = J_{1'2'} + J_{2''2'} + J_{3'2'}$.

Because each of the H1′ resonances is resolved in the one-dimensional NMR spectrum (Figure 2c), each $J_{\Sigma 1'}$ value can be measured trivially. The $J_{1'2'}$ and $J_{1'2''}$ values were measured from standard decoupling experiments; i.e., $J_{1'2'}$ for C3 was measured by decoupling C3-H2″ (Figure 2a) and $J_{1'2''}$ was measured by decoupling C3-H2′ (Figure 2b).

Figure 2c also shows the H2′/H2″ region of the NMR spectrum, which is clearly too crowded to measure the $J_{\Sigma 2'}$ or the $J_{\Sigma 2''}$ values. Thus, a two-dimensional phase-sensitive COSY experiment (Ernst et al., 1987) was used to obtain these parameters. Density matrix theory can be used to show that a COSY cross-peak contains both active and passive couplings (Ernst et al., 1987). For example, an H1′/H2′ cross-peak contains both the active H1′/H2′ coupling and the passive H1′/H2″ coupling. Theory also shows that active couplings are antiphase in nature while passive couplings are in-phase.

Figure 3 shows slices through the C3-H1′/C3-H2′ and C3-H1′/C3-H2″ cross-peaks from the COSY spectrum of $d(C_3G_3)$ at 18 °C. Because both active and passive couplings contribute to a cross-peak, the width between the outermost peaks of the multiplet represents a sum of coupling constants. In Figure 3a, C3-$J_{\Sigma 2'}$ and C3-$J_{\Sigma 2''}$ are observed. In Figure 3b, C3-$J_{\Sigma 1'}$ is observed in either slice, and C3-$J_{1'2'}$ and C3-$J_{1'2'}$ can be extracted as the appropriate active or passive coupling. Thus, these values can be cross-checked with those obtained by one-dimensional methods.

A danger exists in measuring coupling constant values when the $J$ value is not substantially larger then the line width of the multiplet peaks. In the case of an antiphase cross-peak,

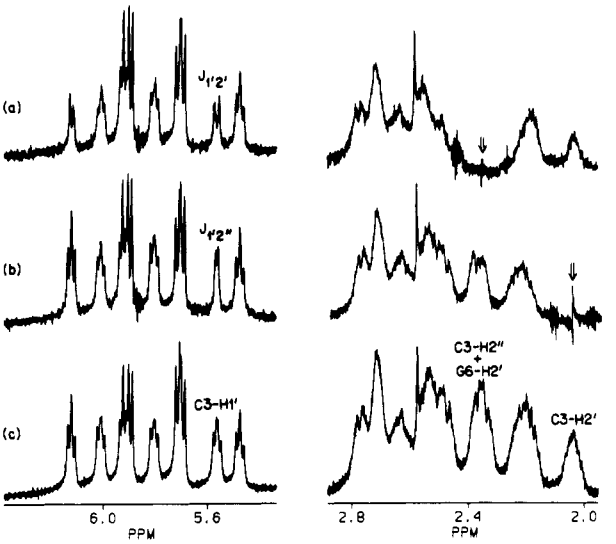


FIGURE 2: Proton homonuclear decoupling experiments on $d(C_3G_3)$ in 100 mM NaCl buffer, 18 °C. (a) The C3-H2″ (and the overlapping G6-H2″) resonances are decoupled, and C3-$J_{1'2'}$ is observed. (b) The C3-H2′ resonance is decoupled, and the C3-$J_{1'2''}$ is observed. (c) Control spectrum.

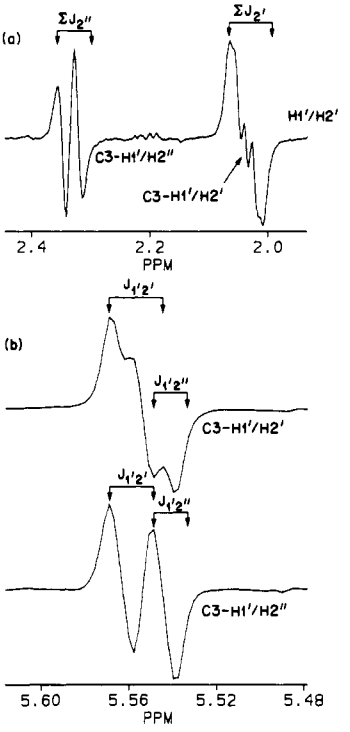


FIGURE 3: Slices from the 500-MHz proton COSY spectrum of $d(C_3G_3)$ in 100 mM NaCl buffer, 18 °C, through the C3-H1′/H2′ and C3-H1′/H2″ cross-peaks. (a) Slice through the C3-H1′ diagonal peak. (b) Slices through the C3-H2′ and C3-H2″ diagonal peaks.

cancellation in the central region causes the apparent extrema to be further apart than the true extrema. For in-phase splittings, the apparent coupling is too small. Thus, all slices were viewed in the $t_2$ dimension, where a larger number of data points (i.e., a less truncated FID) results in narrower line widths. In addition, large error bars were chosen to account for this effect.

The important parameters and corresponding experimental values for each nucleotide are listed in Table II. The method of Rinkel et al. (1987) was then used to determine $P$ values. A brief description of this method follows. Coupling constant values were determined as a function of dihedral angles from a modified Karplus equation. Empirical constants for the

Table II: Coupling Constant Data for the Deoxyribose Protons of d($C_3G_3$) (3 mM) in 100 mM NaCl, 10 mM Sodium Phosphate, pH 7, and 1 mM EDTA at 18 °C

| | C1 | C2 | C3 | G4[a] | G5 | G6 | error |
|---|---|---|---|---|---|---|---|
| $J_{\Sigma 1'}$[b] | 13.4 | 13.4 | 15.0 | 15.3 | 14.4 | 13.4 | ±0.2 |
| $J_{1'2'}$ | 7 | 9 | 9 | | 9 | 8 | ±1 |
| $J_{1'2''}$ | 5 | 5 | 5 | | 4 | 5 | ±1 |
| $J_{\Sigma 2'}$[c] | 26 | 27 | 28 | | 27 | 28 | ±2 |
| $J_{\Sigma 2''}$[d] | 24 | 21 | 21 | | 22 | 22 | ±2 |
| % south | 70 | 80 | >90 | >90 | 85 | 70 | ±10 |
| $P_{south}$[e] (deg) | 185 | 195 | 195 | 185 | 195 | 195 | ±15 |

[a] G4-H2′ and G4-H2″ have the same chemical shift. [b] $J_{\Sigma 1'} = J_{1'2'} + J_{1'2''}$. [c] $J_{\Sigma 2'} = J_{1'2'} + J_{2'2''} + J_{2'3'}$. [d] $J_{\Sigma 2''} = J_{1'2''} + J_{2'2''} + J_{2''3'}$. [e] For B-form, $P = 162°$; for A-form, $P = 18°$.

modified Karplus equation were determined from a least-squares fit of a data set of 315 molecules for which dihedral angles and NMR coupling constants were known (Haasnoot et al., 1980). These constants could reproduce the data set with an root mean square deviation of 0.5 Hz. By use of this equation, graphs of proton–proton coupling constants (and sums of coupling constants) as a function of $P$ were generated for deoxyribose. A $P$ value is then sought for which all experimental and theoretical coupling constant values matched within experimental error. If no reasonable fit was found, a north/south equilibrium was presumed. Because the conformations are predominantly southern, the northern conformation was fixed at C3′-endo ($P = 18°$), and the percent contribution and the conformation in the southern range were varied.

The best fits for the data on d($C_3G_3$) are listed in Table II. The data show a clear predominance of southern (B-like) deoxyribose conformations. The pseudorotation phase angles, however, are not C2′-endo ($P = 162°$) as would be expected in standard B-form geometry. The dominant conformer is closer to C3′-exo ($P = 198°$) or C3′-exo/C2′-endo ($P = 180°$). The percent contribution from northern (A-like) conformers gets larger toward the ends of the helix. Even greater effects of this type have been previously observed in d(GGATGGGAG)·d(CTCCCATCC), where the terminal cytosines were only 40% south (Aboul-ela et al., 1988).

The H1′/H5 region of r($C_3G_3$) in 100 mM NaCl buffer at 18 °C is shown in Figure 1. Because the H1′ resonances have the appearance of singlets, $J_{1'2'}$ is ≤1 Hz. This suggests the presence of predominantly C3′-endo ribose conformations, which is consistent with an A conformation in the ribooligonucleotide.

*Interproton Distances.* NOE (Noggle & Schirmer, 1971) experiments were done to calculate interproton distances by using the approximation

$$\sigma_{ij}/\sigma_{kl} = r_{kl}^6/r_{ij}^6 \quad (1)$$

where $\sigma_{ij}$ and $\sigma_{kl}$ are the cross-relaxation rates between two nuclei $i$ and $j$, and $k$ and $l$, respectively, and $r_{ij}$ and $r_{kl}$ are the respective internuclear distances (Wagner & Wüthrich, 1979). This assumption is reasonable when all spin pairs in the molecule have the same effective correlation time. Cross-relaxation rates were estimated from the initial slopes of NOE buildup curves, which plot the magnitude of an NOE vs the time during which the spin pair is allowed to interact (the mixing time). If the cross-relaxation rates are measured for two pairs of spins, one of which is separated by a known fixed distance, then the distance between the second pair can be calculated by using eq 1. The cytosine H6/H5 distance (2.4 Å) and the deoxyribose H2′/H2″ distance (1.8 Å) were used as reference distances. These two references were internally consistent (one correctly predicts the other distance within experimental error), which is consistent with the assumption that a single correlation time dominates the relaxation. Errors in distances were estimated by a propagation of errors as was done by Fesik et al. (1986) and are listed in Table IV.

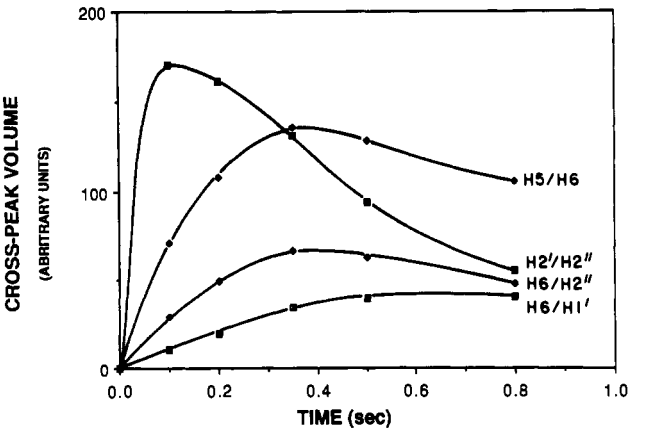


FIGURE 4: Some of the intranucleotide NOE buildup curves from the C3 nucleotide of d($C_3G_3$) in 100 mM NaCl buffer, 18 °C. Cross-peak intensities were integrated from NOESY spectra with mixing times of 100, 200, 350, 500, and 800 ms. A relaxation delay of 6 s was used.

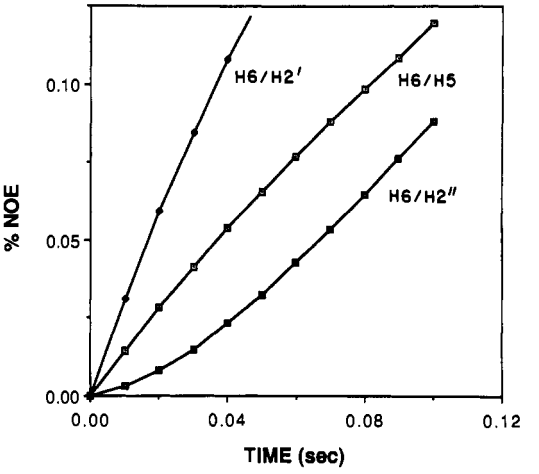


FIGURE 5: Theoretical NOE buildup curves generated for four spins (H6, H5, H2′, and H2″) of a cytidine nucleotide in B-form geometry. Positive curvature of the H6/H2″ curve demonstrates a contribution from spin diffusion. Table III shows how this affects distance estimates.

NOE intensities for all spin pairs at a particular mixing time were collected simultaneously by using the two-dimensional NOESY experiment (Ernst et al., 1987) and were measured as cross-peak volumes. Figure 4 shows a plot of some of the C3 intraresidue NOE buildup curves. This figure shows the importance of using short mixing times to estimate cross-relaxation rates. Calculations show that mixing times below 200 ms must be used to obtain internally consistent values for the two fixed distances. For longer distances, longer mixing times are also reasonable; however, spin diffusion (Ernst et al., 1987) begins to add a confounding variable. For example, the NOE between cytosine H6 and H2″ protons can be short-circuited by the H2′ proton, which is located somewhat between the other two. Consequently, the H6/H2″ buildup will be faster than that of the isolated spin pair and the distance will be underestimated. With these considerations in mind, NOESY experiments with mixing times of 35, 70, and 105 ms were used to calculate cross-relaxation rates.

Theoretical calculations show that for the H6 → H2′ → H2″ spin diffusion pathway, which represents one of the worst possible scenarios in DNA, even these experimental mixing

Table III: Distance Predictions Using Equation 1 and Theoretical Buildup Curves (Figure 5)[a]

| $\sigma_{theoretical}$ ($s^{-1}$) | $r$ (Å) | $\sigma_{theoretical}$ ($s^{-1}$) | calculated distance (Å), from slope measured through time points up to | | | |
|---|---|---|---|---|---|---|
| | | | 10 ms | 30 ms | 100 ms | 250 ms |
| H5/H6 | 2.4 | 1.48 | | | | |
| H6/H2′ | 2.1 | 3.30 | 2.1 | 2.1 | 2.2 | 2.3 |
| H6/H2″ | 3.4 | 0.18 | 3.3 | 2.9 | 2.6 | 2.4 |

[a] Curves were generated for each spin pair; slopes were measured, and distances were calculated by using the H5/H6 slope ($\sigma_{apparent}$) as a reference. $\sigma$ values were calculated as a linear least-squares fit slope through the points up to that time value.

times are too long. Figure 5 shows theoretical buildup curves corresponding to short mixing times for a four-spin system designed to mimic the cytidine H6, H5, H2′, and H2″ protons in B-form geometry. The curves were generated by numerically integrating a modified form of the Bloch equations:

$$dM_i/dt = \rho_i(M_i - M_{i0}) + \sum\sigma_{ij}(M_j - M_{j0}) + \sigma_{ik}M_k$$

where $M_{i0}$ represents the equilibrium magnetization of spin $i$ and $\rho$ and $\sigma$ have the usual definitions (Abragam, 1961; Kearns, 1984; Lane et al., 1986). A fourth-order Runge–Kutta algorithm was used for the integration. For this example, the H6 proton was irradiated, and NOEs at the remaining spins were observed as a function of the mixing time. A correlation time of 5 ns was assumed, and the H5/H6 buildup rate was used as a reference for the distance calculations.

The positive curvature that appears around 20 ms in the H6/H2″ buildup indicates that this cross relaxation becomes dominated by a spin diffusion pathway, in this case H6 → H2′ → H2″. Due to the small magnitude of the NOEs at these mixing times, the onset of spin diffusion is difficult to detect in experimental data, and the usual tendency is to take the initial slope through the data points. Table III shows how the calculated distance varies as a function of the longest time point used in the calculation. In each case $\sigma$ is taken as the slope of a linear least-squares fit through the data points up to that time point. Clearly, only data below 10 ms give accurate distance estimates, though this time limit is sensitive to the correlation time chosen. Because the NOEs are less than 2%, 10 ms is too short to get sufficient signal to noise to accurately integrate cross-peaks. Thus, accurate H6/H2″ distances could not obtained by this method. Similar calculations show that the H6/H1′ distance can be accurately measured by using data extending out to about 30 ms. Thus, these distances were calculated by using the 35-ms NOESY experiment only. It is clear that the nature of the spin system (i.e., spin diffusion pathways) must always be considered in order to evaluate distance estimates.

Intranucleotide distances calculated by using eq 1 are listed in Table IV-A. Some distances could not be obtained due to spectral overlap. As mentioned, the H6(8)/H2″ distances are likely to be underestimated. Intraresidue distances were compared to maps that plot these distances as a function of the pseudorotation phase angle ($P$) and the glycosidic torsion angle ($\chi$) of the residue (Wüthrich, 1986). The ranges of $P$ and $\chi$ that are consistent with all of the calculated distances are shown in Table IV. The error bars listed for $\chi$ and $P$ represent the range of overlap of all intraresidue distance measurements. It should be noted that certain distances are far more sensitive to structural changes than others. For example, the H2′/H4′ distance varies between 2.3 and 3.9 Å as a function of $P$, while the H1′/H2′ distance varies between 2.1 and 2.2 Å. The first difference is detectable by NOE measurements, while the latter is not. $P$ values are consistent with those obtained from the coupling constant data but are not as tightly constrained. $\chi$ values are all in the range for B-family structures. Only C2 has the A-form value within its experimental error range.

Experimental NMR internucleotide distances are tabulated in Table IV-C; A- and B-form distances are included for comparison. The measured distances are not uniformly consistent with either A- or B-form structures, and spin diffusion cannot explain the discrepancies. This suggests that the internucleotide geometry is neither A- or B-form; it is inter-

Table IV: Proton–Proton Distances[a] within d($C_3G_3$) (3 mM) in 100 mM NaCl, 10 mM Sodium Phosphate, pH 7, and 1 mM EDTA at 18 °C

(A) Intranucleotide Distances

| | C1 | C2 | C3 | G4 | G5 | G6 |
|---|---|---|---|---|---|---|
| H6(8)/H1′ | | 3.3 | 3.2 | 3.4 | 3.3 | 3.1 |
| H6(8)/H2′ | 2.9 | 2.1 | 2.1 | | | |
| H6(8)/H2″ | 2.7[b] | 2.7[b] | 2.8[b] | | | 2.9[b] |
| H6(8)/H3′ | 3.5 | | 3.6 | 3.5 | 3.1 | 3.5 |
| H6(8)/H4′ | | 4.9 | | | | |
| H1′/H2′ | 2.7 | 2.9 | 2.9 | | 2.8 | 2.6 |
| H1′/H2″ | 2.3 | 2.3 | 2.3 | | 2.3 | 2.3 |
| H1′/H3′ | 3.4 | | | | 3.7 | 3.9 |
| H1′/H4′ | 3.6 | 3.4 | 3.6 | 3.0 | 3.2 | 3.3 |
| H2′/H3′ | 2.4 | | | | 2.2 | |
| H2′/H4′ | | 3.8 | | | 3.4 | 2.9 |
| H2″/H3′ | | | | | 2.2 | 2.6 |
| H2″/H4′ | 3.0 | | 3.3 | | 3.5 | 3.7 |

(B) Analysis of Intranucleotide Distances

| | C1 | C2 | C3 | G4 | G5 | G6 | A-form | B-form |
|---|---|---|---|---|---|---|---|---|
| $P$ (deg) | 175 ± 25 | 190 ± 40 | 195 ± 45 | ≈170 | 195 ± 45 | 175 ± 25 | 18 | 162 |
| $\chi$ | −115 ± 5 | −140 ± 30 | −90 ± 30 | −105 ± 45 | −90 ± 30 | −90 ± 30 | −170 | −100 |

(C) Internucleotide Distances

| $n/(n-1)$ | G6 → G5 | G5 → G4 | G4 → C3 | C3 → C2 | C2 → C1 | A-form | B-form[c] |
|---|---|---|---|---|---|---|---|
| H2′/H1′ | 3.7 | | | | | >5.0 | >5.0 |
| H6(8)/H1′ | | | 3.3 | 3.4 | 3.8 | 4.6 | 3.5 |
| H6(8)/H2′ | | >3.0[d] | 3.6 | 3.0 | | 2.0 | 3.9 |
| H6(8)/H2″ | | >3.0[d] | 3.3 | 2.8 | 2.8 | 3.8 | 2.2 |

[a] All distances are in angstroms. Distance errors are approximately ±0.2 Å for 2.0–2.5 Å; ±0.3 Å for 2.5–3.0 Å; ±0.4 Å for 3.0–3.5 Å; ±0.7 Å for 3.5–4.0 Å; and ±1.0 Å for 4.0–5.0 Å. [b] These distances are probably underestimated (see text). [c] A- and B-form parameters are from Wüthrich (1986). [d] Approximate distances due to overlapping cross-peaks.

Table V: Parameters from Molecular Mechanical Studies[a]

| | sugar phase ($P$) (deg) | | | energy (kcal mol$^{-1}$) | |
|---|---|---|---|---|---|
| | initial | final range | axis offset ($D$) (Å) | initial | final |
| A-form | 12 | 14, 18, 18, 18, 15, 19<br>14, 18, 18, 18, 15, 19 | 3.6–4.1 | 2900 | −500 |
| | 175 | 164, 116, 78, 15, 12, 158<br>175, 78, 150, 20, 13, 161 | 3.6–4.6 | 710000 | −500 |
| B-form | 175 | 171, 172, 172, 177, 176, 182<br>171, 172, 172, 177, 176, 182 | −0.4 to −1.1 | 730 | −520 |
| | 12 | 76, 120, 110, 130, 130, 74<br>75, 120, 109, 128, 128, 71 | −0.6 to −1.6 | 6800 | −480 |

[a] The pseudorotation phase angle $P$ and the helix displacement parameter $D$ are presented. Each row of $P$ values presents one strand of the $d(C_3G_3)$ double helix in the 5′ to 3′ direction.

mediate, but biased toward B-form. Whether this is due to a stable intermediate conformation or a dynamic equilibrium is unclear.

*Circular Dichroism.* Circular dichroism, the differential absorption of right and left circularly polarized light, is sensitive to the base-stacking geometry in nucleic acids. The CD spectrum of $d(C_3G_3)$ in 100 mM NaCl buffer (pH 7) obtained as a function of temperature is shown in Figure 6a. The maximum at 259 nm and the 1.9 to −1.0 intensity ratio of the bands at 259 and 234 nm, respectively, are consistent with CD spectra of polydeoxynucleotides (presumed B-form) containing nearest-neighbor GC base pairs (Gray et al., 1978). The minimum at 282 nm is unusual and was found to be pH sensitive; the intensity of the band was nearly zero at pH 5.5 (data not shown). The two isosbestic points at 248 and 271 nm are consistent with a two-state transition and suggest that this unusual band is not due to an aggregated state. The highest temperature spectrum (65 °C) is characteristic of a single-stranded structure, which is consistent with results from absorbance thermal denaturation studies.

The CD spectrum of $r(C_3G_3)$ in the same buffer at 18 °C is shown in Figure 6b. The RNA structure is presumed to be A-form, on the basis of NMR coupling constant and chemical shift data (see above). Here, the maximum has shifted to 267, and the 267 nm to 234 nm ratio has increased to 3.1 to −1.0. There is also a minimum at 292 nm.

To test the possibility that $d(C_3G_3)$ has A-like stacking, trifluoroethanol (TFE), which is known to induce a B to A transition in DNA oligo- and polynucleotides, was added. Figure 6c shows the CD spectra of $d(C_3G_3)$ in 2 mM NaCl at 8 °C containing 0% and 80% TFE by volume. The low-salt condition was used to minimize precipitation and/or aggregation of the DNA in the presence of TFE. The lower temperature was used to partially offset the decrease in melting temperature found upon addition of TFE. Under these conditions, absorbance studies show that approximately 25% of the molecules were single stranded at 8 °C. The similarity of the 0% TFE spectrum and the 100 mM NaCl buffer spectrum at 18 °C indicates that the change in salt conditions did not significantly alter the average structure. In 80% TFE, the CD spectrum becomes very similar to the RNA spectrum. The band at 282 nm disappears completely; therefore, it is not due to base stacking similar to the A-form. The bands in the 80% TFE spectrum are less intense than those in the RNA spectrum and are likely to be due to contributions from single strands.

*Molecular Mechanics Studies.* The possibility that B-like deoxyribose conformations can be accommodated in an A-form stacking arrangement without a significant energy cost was investigated by molecular mechanics studies using AMBER (Kollman et al., 1981). The case of A-like sugars in B-form stacking was also studied. The results are shown in Table V,

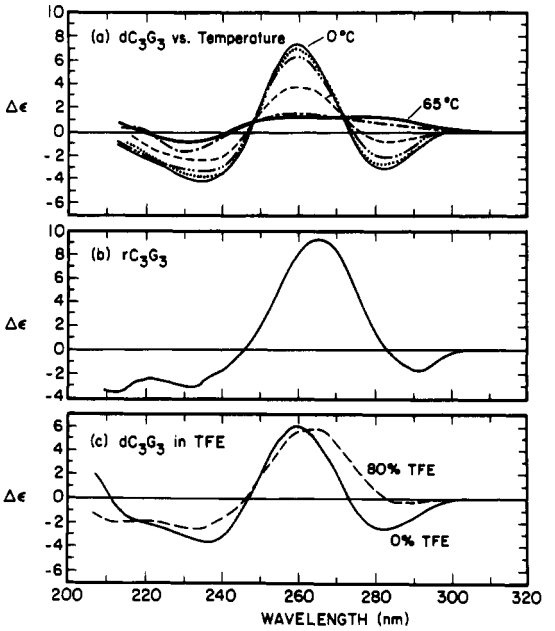


FIGURE 6: CD spectra of (a) $d(C_3G_3)$ in 100 mM NaCl buffer as a function of temperature (0–65 °C), (b) $r(C_3G_3)$ in 100 mM NaCl buffer, 18 °C, and (c) $d(C_3G_3)$ in 2 mM NaCl, pH 7, 8 °C, at 0% and 80% trifluoroethanol (by volume). The intensity of the 80% TFE spectrum was not corrected for the single-stranded contribution.

along with the pseudorotation phase angles ($P$) and helix displacement parameters [$D$; see Saenger (1984)] of each final structure. The molecular mechanical energies of all the minimized structures were within 20 kcal of −500 kcal mol$^{-1}$, indicating that the minimized modified structures are energetically comparable to the standard forms. The base stacking geometries of the modified structures were similar to their unmodified counterparts, as judged by the $D$ values (Saenger, 1984). To determine whether the small energy difference between minimized standard A- and B-forms was sequence-dependent, d(GATCAC)·d(GTGATC) was also energy minimized in the A and B conformations, yielding energies of −440 and −450 kcal mol$^{-1}$, respectively. The A/B difference in this case is comparable to that for $d(C_3G_3)_2$.

The $P$ values for the initial and energy-minimized structures are listed in Table V. The four internal nucleosides, whose conformations are least perturbed by end effects and should be most characteristic of actual nucleic acids, will be discussed. When B-like sugars ($P$ = 175°) are initially placed in an A-form structure, the energy is extremely high. After minimization the final energy is similar to the energy of the minimized standard A-form. The internal nucleosides of the final structure have a large range of $P$ values ($P$ = 12–150°). The two internal guanosines in each strand have A-like (C3′-endo) sugars, but the internal pyrimidine nucleosides remain B-like (C2′-endo to O4′-endo). In contrast, when

A-like sugars ($P$ = 12°) are initially placed in a B-form structure, the internal nucleosides of the final structure have a narrower range of $P$ values ($P$ = 109–130°). The four inner nucleosides are approximately C1′-exo, close to the B-form C2′-endo.

It should be noted that the introduction of a different deoxyribose pucker into an otherwise standard helical conformation is accompanied by perturbation of the backbone structure. This is evidenced by the high energies of the initial structures (Table V), particularly when B-type sugars are placed in an A-form structure. Because of the manual method by which this was done, the perturbations were not regular from one nucleotide to the next. Consequently, each modified structure must be viewed as one possibility from a potentially large range. Nevertheless, the results show qualitatively that B-type deoxyribose conformations can be accommodated in one strand of an A-form duplex without significant energetic destabilization.

## Discussion

The primary conclusion from these results is that under mild aqueous solvent conditions the solution structure of d($C_3G_3$) is neither standard A- or B-form geometry but is certainly a B-type structure. The relative chemical shifts of the CH6 and GH8 resonances for d($C_3G_3$) are different than for r($C_3G_3$), suggesting that the stacking geometry in d($C_3G_3$) is not A-like. Coupling constant data are consistent with predominantly C3′-exo ($P$ = 198°) or C3′-exo/C2′-endo ($P$ = 180°) deoxyribose conformations. These southern conformations are similar, but not equivalent to B-form pucker (C2′-endo, $P$ = 162°), and are significantly different from that of A-form (C3′-endo, $P$ = 18°). Intranucleotide proton–proton distances obtained from NOE experiments support this conclusion but present larger uncertainty limits. These same distances indicate glycosidic torsion angle limits that include B-form and exclude A-form. Internucleotide proton–proton distances are indicative of a structure that is intermediate between these extremes but is closer to B-form. It is useful to compare our results with those of Fratini et al. (1982) obtained in their study of the B-DNA dodecanucleotide d(CGCGAATTCGCG). They found that the sugar puckers varied over the entire range from C2′-endo ($P$ = 162°) to C3′-endo ($P$ = 18°). We observed a much smaller range of sugar puckers (175° < $P$ < 195°) for d($C_3G_3$) in solution (Tables II and IV-B).

Circular dichroism spectra for d($C_3G_3$) have characteristics expected from the circular dichroism spectra of B-type polydeoxynucleotides containing d(GG)·d(CC) and d(CG)·d(CG) sequences (Gray et al., 1978). The spectra are different from the CD of the same sequence RNA and can be shifted to an A-type RNA spectrum by adding trifluoroethanol, which is known to induced B-to-A transitions. The CD indicates that the base stacking in d($C_3G_3$) is clearly different from that in r($C_3G_3$), but it cannot reveal more without detailed calculations of the spectra.

Molecular mechanics energy-minimization studies showed that in an A-type stacking arrangement cytidines can exist with B-type sugar conformations without significant destabilization. In contrast, the sugar puckers were all B-family (O4′-endo to C2′-endo) with B-type stacking.

The spectroscopic results indicate that d($C_3G_3$) adopts a "B-family" structure with nonstandard deoxyribose conformations and internucleotide stacking geometry. Whether more detailed analysis, such as the use of NMR distance–geometry (Hare & Reid, 1986; Crippen, 1981), can reveal particular subtle structural shifts such as base roll and base slide in detail remains to be seen. These data do, however, emphasize the difference between the results of X-ray crystallographic and solution NMR studies. The difference may be due to a structural change induced by the conditions required for crystal formation. Clearly, a combination of the two techniques will usually be more informative than either method alone.

The structural deviations from B-form reported here are not large, but it is possible that they amount to significant helix perturbation when propagated through a long run of identical residues. Such a perturbation could be involved in protein recognition. In addition, the biological environment, such as superhelical stress or protein binding, can induce further changes in conformation. It is clearly important to recognize the wide range of conformations that DNA can take up as a function of sequence and environment.

## Acknowledgments

We gratefully acknowledge Dr. Jamie Williamson for providing the plans to build the DNA synthesizer and Peter Davis for many useful discussions about RNA synthesis.

**Registry No.** d$C_3G_3$, 81994-17-4; r$C_3G_3$, 118418-99-8.

## References

Aboul-ela, F., Varani, G., Walker, G. T., & Tinoco, I., Jr. (1988) *Nucleic Acids Res. 16*, 3559–3572.

Abragam, A. (1961) *Principles of Nuclear Magnetism*, pp 289–305, Oxford University Press, Oxford.

Altona, C., & Sundaralingam, M. (1972) *J. Am. Chem. Soc. 94*, 8205–8212.

Benevides, J. M., Wang, A. H.-J., Rich, A., Kyogoku, Y., van der Marel, G. A., van Boom, J. H., & Thomas, G. J., Jr. (1986) *Biochemistry 25*, 41–50.

Bodenhausen, G., Kogler, H., & Ernst, R. R. (1984) *J. Magn. Reson. 58*, 370–388.

Calladine, C. R. (1982) *J. Mol. Biol. 161*, 343–352.

Conner, B. N., Takano, T., Tanaka, S., Itakura, K., & Dickerson, R. E. (1982) *Nature 295*, 294–298.

Crippen, G. M. (1981) *Distance Geometry and Conformational Calculations*, Research Studies Press/Wiley, Chichester.

de Leeuw, F. A. A. M., & Altona, C. (1982) *J. Chem. Soc., Perkin Trans. 2*, 375–384.

Ernst, R. R., Bodenhausen, G., & Wokaun, A. (1987) *Principles of Nuclear Magnetic Resonance in One and Two Dimensions*, Chapters 8 and 9, Clarendon Press, Oxford.

Fesik, S. W., O'Donnell, T. J., Gampe, R. T., Jr., & Olejniczak, E. T. (1986) *J. Am. Chem. Soc. 108*, 3165–3170.

Fratini, A. V., Kopka, M. L., Drew, H. R., & Dickerson, R. E. (1982) *J. Biol. Chem. 257*, 14686–14707.

Giessner-Prettre, C., & Pullman, B. (1970) *J. Theor. Biol. 27*, 87–95.

Giessner-Prettre, C., & Pullman, B. (1976) *Biopolymers 15*, 2277–2286.

Gray, D. M., Hamilton, F. D., & Vaughn, M. R. (1978) *Biopolymers 17*, 85–106.

Haasnoot, C. A. G., de Leeuw, F. A. A. M., & Altona, C. (1980) *Tetrahedron 36*, 2783–2792.

Haran, T. E., Shakked, Z., Wang, A. H.-J., & Rich, A. (1987) *J. Biomol. Struct. Dyn. 5*, 199–217.

Hare, D. R., & Reid, B. R. (1986) *Biochemistry 25*, 5341–5350.

Hare, D. R., Wemmer, D. E., Chou, S.-H., Drobny, G., & Reid, B. R. (1983) *J. Mol. Biol. 171*, 319–336.

Heinemann, U., Lauble, H., Frank, R., & Blocker, H. (1987) *Nucleic Acids Res. 15*, 9531–9551.

Karplus, M. (1959) *J. Chem. Phys. 30*, 11–15.
Kearns, D. R. (1984) *CRC Crit. Rev. Biochem. 15*, 237–290.
Kierzek, R., Caruthers, M. H., Longfellow, C. E., Swinton, D., Turner, D. H., & Freier, S. M. (1986) *Biochemistry 25*, 7840–7846.
Kollman, P., Weiner, P., & Dearing, A. (1981) *Biopolymers 20*, 2583–2621.
Lane, A. N., Lefevre, J.-F., & Jardetzky, O. (1986) *J. Magn. Reson 66*, 201–218.
Markiewicz, W. T., Biala, E., & Kierzek, R. (1984) *Bull. Pol. Acad. Sci., Chem. 32*, 433.
McCall, M., Brown, T., & Kennard, O. (1985) *J. Mol. Biol. 183*, 385–396.
Nickol, J. M., & Felsenfeld, G. (1983) *Cell 35*, 467–477.
Nishimura, Y., Torigoe, M., & Tsuboi, M. (1985) *Biopolymers 24*, 1841–1844.
Noggle, J. H., & Schirmer, R. E. (1971) *The Nuclear Overhauser Effect: Chemical Applications*, Chapter 1, Academic Press, New York.
Otting, G., Widmer, H., Wagner, G., & Wüthrich, K. (1986) *J. Magn. Reson. 66*, 187–193.
Patel, D. J., Canuel, L. L., & Pohl, F. M. (1979) *Proc. Natl. Acad. Sci. U.S.A. 76*, 2508–2511.
Rhodes, D. (1979) *Nucleic Acids Res. 6*, 1805–1815.
Rinkel, L. J., & Altona, C. (1987) *J. Biomol. Struct. Dyn. 4*, 621–649.
Sanger, W. (1984) *Principles of Nucleic Acid Structure*, pp 22 and 287, Springer-Verlag, New York.
Schon, E., Evans, T., Welsh, J., & Efstratiadis, A. (1983) *Cell 35*, 837–848.
Simpson, R. T., & Künzler, P. (1979) *Nucleic Acid Res. 6*, 1387–1415.
Ti, G. S., Gafney, B. L., & Jones, R. A. (1982) *J. Am. Chem. Soc. 104*, 1316.
Wagner, G., & Wüthrich, K. (1979) *J. Magn. Reson. 33*, 672–680.
Wang, A. H.-J., Fulfii, S., van Boom, J. H., & Rich, A. (1982) *Proc. Natl. Acad. Sci. U.S.A. 79*, 3968–3972.
Weiner, S. J., Kollman, P. A., Singh, U. C., Ghio, C., Alagona, G., Profeta, S., & Weiner, P. K. (1984) *J. Am. Chem. Soc. 106*, 765–784.
Wells, R. D., Blakesly, R. W., Hardies, S. C., Horn, G. T., Larson, J. E., & Selsing, E. (1977) *CRC Crit. Rev. Biochem. 4*, 305–340.
Wüthrich, K. (1986) *NMR of Proteins and Nucleic Acids*, pp 203–223, John Wiley & Sons, New York.

# Formylglycinamide Ribonucleotide Synthetase from *Escherichia coli*: Cloning, Sequencing, Overproduction, Isolation, and Characterization[†,‡]

F. J. Schendel, E. Mueller, and J. Stubbe*
*Department of Chemistry, Massachusetts Institute of Technology, Cambridge, Massachusetts 02139*
A. Shiau and J. M. Smith
*Seattle Biomed Research Institute, Seattle, Washington 98109-1651*
*Received July 12, 1988; Revised Manuscript Received November 22, 1988*

ABSTRACT: The *pur*L gene of *Escherichia coli* encoding the enzyme formylglycinamidine ribonucleotide (FGAM) synthetase which catalyzes the conversion of formylglycinamide ribonucleotide (FGAR), glutamine, and MgATP to FGAM, glutamate, ADP, and $P_i$ has been cloned and sequenced. The mature protein, as deduced by the structural gene sequence, contains 1628 amino acids and has a calculated $M_r$ of 141 418. Comparison of the *pur*L control region to other pur loci control regions reveals a common region of dyad symmetry which may be the binding site for the "putative" repressor protein. Construction of an overproducing strain permitted purification of the protein to homogeneity. N-Terminal sequence analysis and comparison of glutamine binding domain sequences (Ebbole & Zalkin, 1987) confirm the amino acid sequence deduced from the gene sequence. The purified protein exhibits glutaminase activity of 0.02% the normal turnover, and $NH_3$ can replace glutamine as a nitrogen donor with a $K_m$ = 1 M and a turnover of 3 $min^{-1}$ (2% glutamine turnover). The enzyme forms an isolable (1:1) complex with glutamine: $t_{1/2}$ is 22 min at 4 °C. This isolated complex is not chemically competent to complete turnover when FGAR and ATP are added, demonstrating that ammonia and glutamine are not covalently bound as a thiohemiaminal available to complete the chemical conversion to FGAM. Hydroxylamine trapping experiments indicate that glutamine is bound covalently to the enzyme as a thiol ester. Initial velocity and dead-end inhibition kinetic studies on FGAM synthetase are most consistent with a sequential mechanism in which glutamine binds followed by rapid equilibrium binding of MgATP and then FGAR. Incubation of [$^{18}$O]FGAR with enzyme, ATP, and glutamine results in quantitative transfer of the $^{18}$O to $P_i$.

Formylglycinamide ribonucleotide (FGAM)[1] synthetase is the fourth step in the purine biosynthetic pathway and catalyzes the irreversible conversion of formylglycinamide ribonucleotide (FGAR), glutamine, and ATP to FGAM, $P_i$, ADP, and glutamate (eq 1). This protein was first purified to homogeneity from *Salmonella typhimurium* by French et al.

[†] This work was supported by Grants GM 32191 (J.S.) and AI 20068 (J.M.S.) from the National Institutes of Health. J.S. is the recipient of a Research Career Development Award (AM 01222) and at MIT is the recipient of the Ellen Swallow Richards Professorship.
[‡] The nucleic acid sequence in this paper has been submitted to GenBank under Accession Number J02848.

[1] Abbreviations: FGAM, formylglycinamidine ribonucleotide; FGAR, formylglycinamide ribonucleotide; HEPES, *N*-(2-hydroxyethyl)-piperazine-*N*′-2-ethanesulfonic acid; SDS, sodium dodecyl sulfate; AIR, aminoimidazole ribonucleotide.

0006-2960/89/0428-2459$01.50/0 